Available online at www.sciencedirect.com
SCIENCE DIRECT®
Thin Solid Films 514 (2006) 132–137
thin solid films
www.elsevier.com/locate/tsf

Multicolor luminescence of undoped zinc sulfide nanocrystalline thin films at room temperature

Baibaswata Bhattacharjee [1], Chung-Hsin Lu *

Electronic and Electro-optical Ceramics Lab, Department of Chemical Engineering, National Taiwan University, Taipei, Taiwan, R.O.C.

Received 19 October 2005; received in revised form 27 February 2006; accepted 27 February 2006
Available online 19 April 2006

Abstract

Thin films containing luminescent undoped zinc sulfide (ZnS) nanoparticles, with and without silica capping, were prepared via a simple method using sol-gel technique. Average particle size changed from 3 to 10 nm for the set of ZnS films and 2.5 to 7 nm for the set of ZnS–SiO_2 films when they were annealed from 473 to 673 K in a step of 50 K. The films containing ZnS nanoparticles without silica capping showed size-dependent blue emission at room temperature. The doublet fine structures in the Photoluminescence (PL) spectra were resolved and a qualitative approach was taken to explain the variation in the PL emission with change in the annealing temperature. The films containing ZnS nanoparticles embedded in silica matrix showed ultra violet (UV) and red emissions upon excitation at different energy levels. The UV emission experienced red shift; whereas, the red emission was found to be blue shifted for the films synthesized at higher annealing temperatures. PL intensity decreased with aging for the films containing ZnS particles without silica capping when they were exposed in relatively humid atmosphere (relative humidity 80%) for 6 weeks. The films containing ZnS particles embedded in silica matrix showed much more stable behavior since the emission intensity practically remained constant with aging and the films also restored their quality when exposed to a humid atmosphere.

Keywords: Nanoparticle; Thin film; Photoluminescence; II–VI semiconductor

1. Introduction

ZnS is a commercially important II–VI semiconductor having a wide optical band gap, rendering it a very attractive material for optical application especially in nanocrystalline form. The size-dependent physical property in this form makes ZnS an active area of extensive research [1–11]. Optical and luminescent properties of nanocrystalline ZnS prepared in the forms of thin film, powder and colloid using different synthesis techniques such as sputtering [1], co-evaporation [2], wet chemical [3–5], sol-gel [6,11] solid state [12], micro-wave irradiation [13,14], ultrasonic irradiation [15] or synthesis under high-gravity environment [16] were studied in detail. Luminescence measurements were identified as one of the most important techniques to reveal the energy structure and surface states of these particles [3]. Localized trap states inside the band gap were studied [17] in detail to recognize the sub-bandgap energy levels. It was found that the defect levels play an important role in determining the luminescence characteristics of the ZnS nanoparticles [18] and most of the nanoparticles exhibit broad and Stokes-shifted luminescence arising from the deep traps of the surface states [1,3]. Only clusters with good surface passivation may show high band-edge luminescence [19]. Visible luminescence from ZnS was achieved mainly by adding appropriate dopants in it [20,21]. Very few studies have reported visible red luminescence from undoped ZnS when capped in some silica matrix [22,23]. Therefore, more investigations are needed to explore the possibility of producing multicolor luminescence from undoped ZnS nanoparticles.

In this study, thin films containing ZnS nanoparticles and composite films of ZnS–SiO_2 (in which the ZnS nanoparticles were embedded in SiO_2 matrix) were prepared adopting sol-gel technique. The ZnS thin films showed size-dependent blue emission; whereas, the ZnS–SiO_2 films showed UV and red emission when excited at different energy levels.

* Corresponding author.
E-mail addresses: baib23@gmail.com (B. Bhattacharjee), chlu@ntu.edu.tw (C.-H. Lu).
[1] Permanent address: Department of Physics, Ramananda College, Bishnupur, Bankura, West Bengal, India-722 122.

0040-6090/$ - see front matter © 2006 Elsevier B.V. All rights reserved.
doi:10.1016/j.tsf.2006.02.096

2. Experimental details

To synthesize the thin films having ZnS nanoparticles embedded in silica matrix, the following method was adopted. A silica sol served as the precursor for the host films was prepared by dissolving tetraethyl orthosilicate, $Si(OC_2H_5)_4$ (TEOS, for synthesis, Merck) in 2-propanol, $(CH_3)_2CHOH$ (GR, Merck) and then adding distilled water in it. Hydrochloric acid (0.1 N; Titrisol, Merck) was used as a catalyst. The volume ratio of water to 2-propanol used in the sol was 1:3. A solution of zinc nitrate, $Zn(NO_3)_2{\cdot}6H_2O$ (Purified, Merck) and thiourea, NH_2CSNH_2 (Pure, Merck) in molar ratio of Zn:S = 1:1 was prepared in 2-propanol and distilled water (volume ratio of 2-propanol to water was 2:1) to use as the source for Zn and S, respectively. The solution containing Zn and S precursors was slowly added into the silica sol under vigorous stirring. The stirring was continued for a further 1–2 h after the completion of the mixing to obtain the final sol for the film fabrication. The equivalent molar ratio of silica to ZnS was 70:30. To prepare ZnS thin film without silica matrix, the silica sol was not added into the solution containing Zn and S precursors.

Thin films were fabricated on properly cleaned quartz glass substrates using a spin coater (Chemat Technology, Model KW-4A) at 3000 rpm. The films were transferred immediately after deposition to an oven (Bae Shye, Model BS-V030) pre-set at the required temperature (flash heating at 473–673 K, with 50 K intervals) in air atmosphere for the nucleation and growth of ZnS nanoparticles in the films. Transmission electron microscopy (TEM) was performed using a Hitachi H-7100 microscope operated at the voltage of 100 kV. Films scratched from the quartz substrate were carefully placed on the carbon coated Cu grid for TEM study. X-ray diffraction (XRD) study was performed in a Seifert 3000P diffractometer using Cu K_α radiation ($\lambda = 0.154056$ nm) as X-ray source at 40 kV, 30 mA. The $\theta/2\theta$ scans were carried out at a scanning speed of 4°/min in the 2θ range of 20° to 70°. The photoluminescence (PL) measurements were performed using a Hitachi F-4500 fluorescence spectrophotometer using Xe lamp as an excitation source.

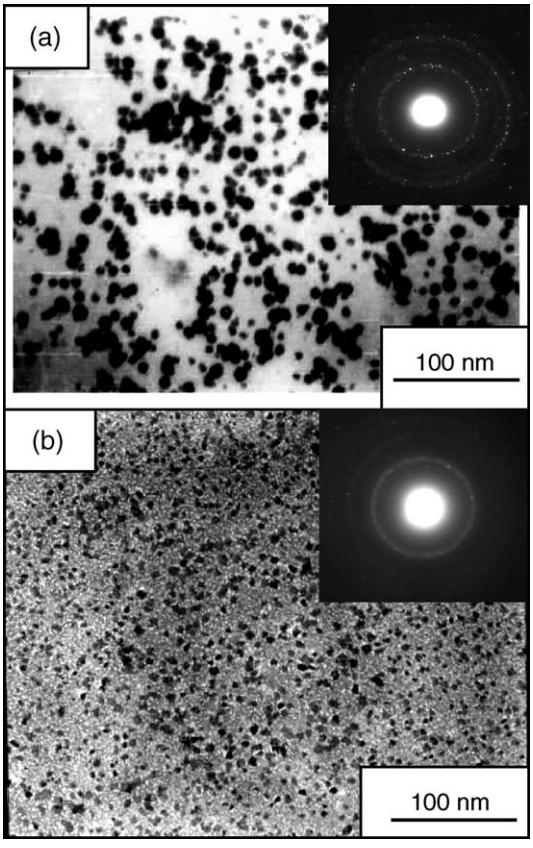

Fig. 1. Transmission electron micrographs (TEM) and corresponding electron diffraction patterns of the films annealed at 673 K for 30 min: (a) thin films containing ZnS nanoparticles without silica matrix and (b) thin films containing ZnS nanoparticles embedded in silica matrix.

Table 1
Comparison in growth of ZnS nanoparticles without and with silica capping against increasing annealing temperature

Annealing temperature (K) [annealing time = 30 min]	Average particle size (nm) [ZnS films]	Average particle size (nm) [ZnS:SiO_2 films]
473	3.0	2.5
523	5.4	4.2
573	7.6	5.7
623	8.9	6.3
673	10.0	7.0

3. Results and discussion

3.1. Microstructural study

Fig. 1(a) and (b) shows respectively the TEM and the corresponding electron diffraction patterns of ZnS and ZnS–SiO_2 films, annealed at 673 K for 30 min. Well dispersed nanoparticles with an average particle size of 10 nm for ZnS and 7 nm for ZnS–SiO_2 films were found under the above mentioned annealing condition. Diffraction patterns showed central halos with concentric ring patterns. Ring patterns showed reflections from (111), (220) and (311) planes, indicating the formation of cubic phase of ZnS in both set of films. Average particle size changed from 3 to 10 nm for the set of ZnS films and 2.5 to 7 nm for the set of ZnS–SiO_2 films when they were annealed from 473 to 673 K in a step of 50 K (Table 1). The full width at half maxima of the particle distribution (data not shown) were changed from 3 to 6 nm for ZnS and from 2 to 4.5 nm for ZnS–SiO_2 set of films when annealed from 473 to 673 K. It was clear from the micrographs that the films containing ZnS nanoparticles without silica capping (Fig. 1a) tend to lose their nanocrystalline nature with increasing annealing temperature at a faster rate when compared to the ZnS–SiO_2 films (Fig. 1b). In the films containing ZnS nanoparticles embedded in silica matrix, the ZnS particles were completely capped inside the silica matrix. The distance among the nanoparticles did not favour the possible coalescence with one another through silica barrier. Thus silica capping made the particles more stable against agglomeration when the annealing temperature was increased.

Fig. 2(a–e) shows the XRD patterns of ZnS–SiO_2 set of films when annealed at different temperatures for 30 min. The

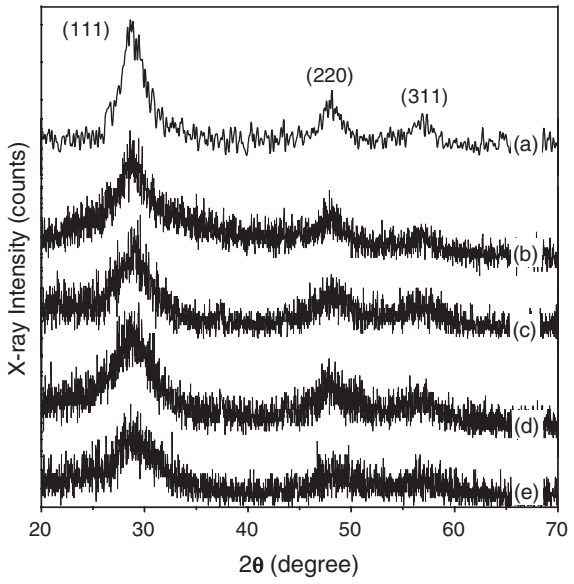

Fig. 2. X-ray diffraction (XRD) patterns of the ZnS–SiO_2 composite films annealed at (a) 673 K, (b) 623 K, (c) 573 K, (d) 523 K and (e) 473 K showing (111), (220) and (311) planes of zinc blend (cubic) structure.

patterns are linearly translated along *Y* axis to avoid overlapping, where the *Y* axis is plotted in linear scale. All films showed peaks from (111), (220) and (311) planes, indicating the formation of a cubic phase, in agreement with the electron diffraction results. The XRD peaks gradually became sharp with increasing annealing temperature indicating the particle growth for higher annealing temperatures.

3.2. PL study of ZnS films

PL spectra of the ZnS nanocrystalline films were recorded at room temperature with an excitation wavelength of 250 nm. Fig. 3(a)–(d) shows the emission spectra of the films annealed at 473, 523, 573 and 673 K respectively. It can be seen (Fig. 3) that the spectral shapes are asymmetric and broad. The peaks are not very smooth having fine structure with a closely separated doublet. The films annealed at lower temperature showed broader PL peak. Shift of these peaks to higher energy levels for the films synthesized at lower annealing temperature (i.e. with smaller crystallite size) was noted for all the films. Several research groups [24–26] studied the blue emission from ZnS nanoparticles under UV excitation. Becker and Bard [24] have attributed the blue emission band at 428 nm to S^{-2} vacancies. Murase et al. [25] ascribed the blue emission band at 470 nm to Zn^{+2} acceptor. Studies conducted by Kanemoto et al. [18] revealed a peak at around 325 nm and ascribed that to the trapped electrons transiting to valance levels. Yanagida et al. [26] have observed defect related longer wavelength luminescence at about 420 nm in addition to the band gap luminescence. Denzler et al. [17] identified four types of point defects, which can be present in pure ZnS generating four trap levels inside the energy gap. Vacancies of zinc and sulphur could be treated as localized acceptor and donor states, whereas, the interstitial atoms of sulphur and zinc led to acceptor and donor states, respectively. That could give rise to four optical transitions — the emissions occurring at longer wavelengths were made associated with the vacancy sites.

In the present work, the PL peaks appeared at energy levels substantially lower than the band gap, suggesting that the transitions from energy states inside the band gap are being favoured for the luminescence process in these nanocrystalline ZnS films. Chen et al. [3] assigned the surface states to the observed PL peak positioned at the energy levels lower than band gap energy and it was also supported by the thermoluminescence measurements made by them. The density of surface states in the nanocrystalline films would increase with a decrease in the size of crystallites constituting the films, due to the increased surface-to-volume ratio in films having smaller crystallites. This would reduce the probability of excitonic emission via non-radiative surface recombination [3,10]. The band-edge or excitonic emission will thus be effectively overlapped with the absorption of the surface states and as such would show photoluminescence at energy levels lower than the band gap.

To resolve the doublet structure and to locate the exact peak positions, each spectrum was deconvoluted as shown in Fig. 3. The experimentally observed spectra could be regarded as the resultant of the contribution from these two peaks. The spectrum corresponding to the film annealed at 473 K for 30 min was deconvoluted into two peaks at 418 and 464 nm. The 418 and 466 nm peaks can be attributed to the S^{-2} vacancy and Zn^{+2} vacancy levels, respectively. Both of these peaks showed gradual red shift with increasing annealing temperature of the films. The model proposed by Chen et al. [3] can explain the size-dependent emission of each component of the PL peaks, i.e. the dependence of emission wavelength on the annealing temperature. With decreasing crystalline sizes, the band gap increases but the trap depth does not change much. Thus the

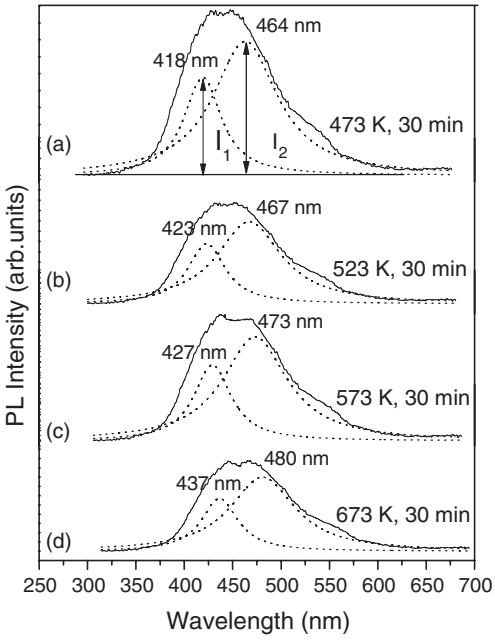

Fig. 3. Photoluminescence (PL) spectra of films containing ZnS quantum dots annealed at (a) 473 K, (b) 523 K, (c) 573 K and (d) 673 K for 30 min.

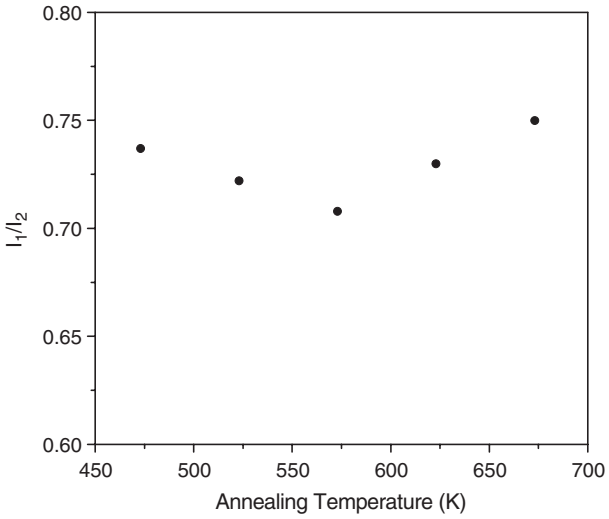

Fig. 4. Change in the ratio of the luminescence intensity of the two peaks originated from Zn^{+2} and S^{-2} vacancy with increasing annealing temperature.

separation between the electron-hole states increases with decreasing size and the luminescence of the surface states shifts to blue. Chestnoy et al. [27] also reported similar type of shift in surface emission dependent on crystallite sizes for CdS nanoclusters.

As the intensity of PL originating from a particular defect level is proportional to the population of that defect site present in the sample, the relative change in PL peak intensity between Zn^{+2} vacancy and S^{-2} vacancy levels with annealing temperature can be explained qualitatively in terms of the change in population of those sites with increasing annealing temperature. Fig. 4 shows the variation of the ratio of the intensities of these two peaks with increasing annealing temperature, where I_1 and I_2 are the luminescence intensities of the peaks due to S^{-2} vacancy and Zn^{+2} vacancy levels respectively as indicated in Fig. 3(a). The peak intensity of the emission originated due to S^{-2} vacancy was always lower than the emission due to Zn^{+2} vacancy because of the fact that S^{-2} vacancy sites were more likely to become passivated by –OH and/or ═O from atmosphere when the films were annealed in air. The intensity ratio decreased primarily due to increasing passivation of S^{-2} vacancy sites by the same process, resulting in lowering PL intensity of the corresponding peak with increasing annealing temperature up to a certain limit. The ratio again increased slightly for the films annealed at higher temperatures. This observation can be attributed to the fact that at higher annealing temperatures, some of the S–Zn bonds on the surface layers of the ZnS particles began to be disrupted and the S atoms broke away from the ZnS and segregated to the film surface. This resulted in an increase in the population of S^{-2} vacancies and led to a corresponding increase in the PL intensity originating from these vacancy sites.

The PL spectra of all the ZnS films showed a weak shoulder around 550 nm. The origin of this shoulder structure at lower energy compared to the main peak can be attributed to the recombination of electron-hole pair at the surface traps, which arise for the high surface to volume ratio of the nanoparticles due to their small sizes. Emission in green region from undoped ZnS was observed by Hu et al. [28] and they assigned the emission to some self-activated centers, probably surface states, vacancy or interstitial states within the structure.

3.3. PL study of ZnS–SiO_2 films

The PL emission spectra of ZnS nanoparticles embedded in the silica matrix were found to be markedly different from those of ZnS particles without silica capping. The ZnS–SiO_2 films showed two PL bands: one in the wavelength range of 350–410 nm and the other in the visible range of 610–652 nm, respectively, when excited at two different energy levels (excitation wavelengths 220 and 380 nm). The blue emission observed in the films containing ZnS nanoparticles without silica capping was absent in the composite ZnS–SiO_2 films. Kumbhojkar et al. [29] observed the UV luminescence generated by the thiol capped ZnS nanocluster, where the emission wavelength varied with different thiols used for capping. On the other hand, Zhu et al. [22] found a PL band in the visible wavelength region of 600–700 nm from undoped ZnS nanoparticles embedded in silica matrices. Cheah et al. [23] managed to generate white luminescence by producing blue and red emissions simultaneously via controlling the amount of nano ZnS doped in porous silicon.

3.3.1. (i) UV emission

Fig. 5(a)–(e) shows the PL emission spectra of the films annealed at different temperatures for 30 min on excitation at 220 nm. The film annealed at 473 K shows its main emission peak at 357 nm, followed by a hump centered at 495 nm. This hump can be attributed to the levels associated with Zn^{+2} vacancy but readily became quenched because of the passivation of the sites due to interaction with the silica matrix as discussed below, when the annealing temperature was

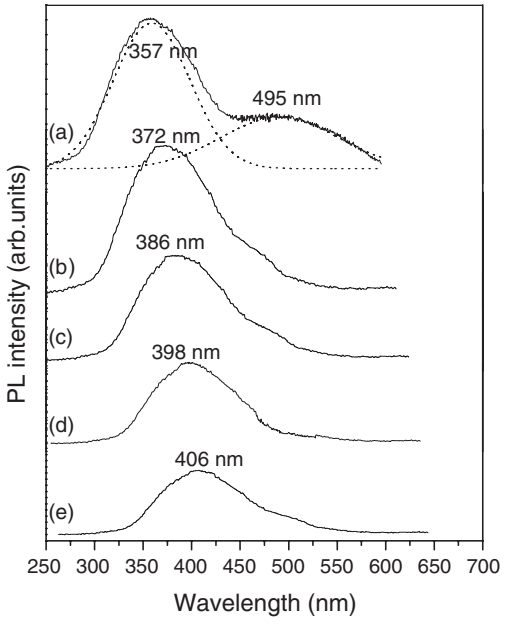

Fig. 5. UV band of the photoluminescence (PL) spectra of films containing ZnS quantum dots embedded in silica matrix, annealed at: (a) 473 K, (b) 523 K, (c) 573 K, (d) 623 K and (e) 673 K for 30 min.

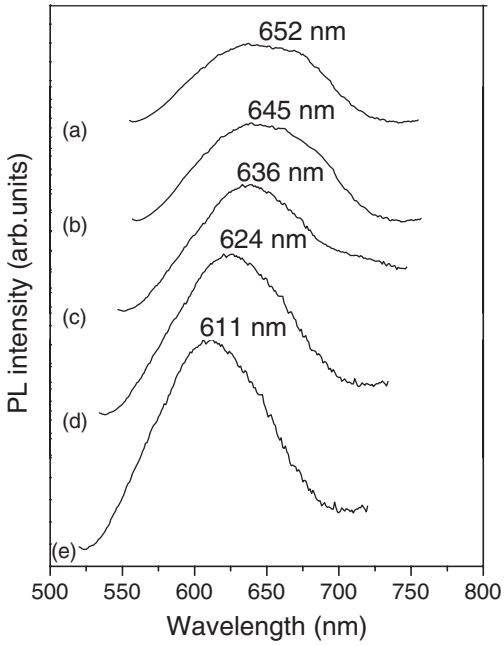

Fig. 6. Red band of the photoluminescence (PL) spectra of films containing ZnS quantum dots embedded in silica matrix, annealed at: (a) 473 K, (b) 523 K, (c) 573 K, (d) 623 K and (e) 673 K for 30 min.

increased. As the annealing temperature was increased to 523 K, the main peak red shifted to 372 nm and the shoulder in the blue region vanishes. This general trend of red shifting of PL peaks with increasing annealing temperature was observed for all the films, and finally the emission peak shifted to 406 nm for the film annealed at 673 K. Gradual decrease in the PL intensity of the films was also observed with increasing annealing temperature.

In the process of hydrolysis and polycondensation of TEOS, the $(OC_2H_5)_3$–Si–O groups got attached to the Zn^{+2} and S^{-2} vacancy sites. Therefore, the traps related to Zn^{+2} and S^{-2} vacancies were removed from the gap and the ligand-terminated surfaces often show deep traps arising due to interstitial Zn or S atoms [17]. Absence of band-edge luminescence and the appearance of broad, red-shifted emission band could be associated to these trap levels. The observed red shift of this emission band with increasing annealing temperature could be explained by the same model proposed by Chen et al. [3] as discussed earlier.

3.3.2. (ii) Red emission

When the films were subjected to 380 nm excitation, visible emission could be observed in the wavelength region of 600–660 nm for the films annealed at different temperatures as shown in Fig. 6(a)–(e). For the film annealed at 473 K for 30 min, the emission spectrum was very broad with the peak around 652 nm. For the film annealed at 523 K for 30 min, the peak appeared around 645 nm and the spectrum became less broad. In case of the films annealed at 573 and 623 K for 30 min, the emission peaks appeared around 636 and 624 nm, respectively. In the above two cases, the line shapes of the spectra were much smoother with a slight asymmetry on the longer wavelength side. The film annealed at 673 K for 30 min emitted around 611 nm upon the same excitation and the spectrum was nearly symmetric with smooth line shape. Intensity of the emission increased gradually with increasing annealing temperature of the films. Red emission from silica coated ZnS nanoparticles and their blue shifting with increasing annealing temperature and/or time were also observed by Zhu et al. [22]. In the present case, the emission spectra were much smooth and defined indicating lesser defects in these sol-gel films compared to the films prepared by laser ablation. Occurrence of this room-temperature red-band luminescence from ZnS nanoparticles embedded in silica matrix, the increasing intensity and blue shifting of this band with increasing annealing temperature could all be explained as a result of increasing occurrence of the S–Zn bond disruption as well as the formation of $ZnS(O_2^-)$ on the surface layers of the ZnS particles [22].

3.4. Study on aging effect

To study the degradation property of the films with time, the luminescence peak intensities of the films relative to that of the freshly prepared samples were investigated as a function of aging time in both sets of films (with and without silica matrix) and the results are shown in Fig. 7 for representative films. Gradual loss in luminescence intensity with aging time was noticed and the luminescence intensity dwindled down to nearly 43% of its initial value for the ZnS films when those are kept in humid air (relative humidity 80%) for 6 weeks, though the emission wavelength didn't experience any noticeable shift. It was noted that the luminescence behavior was much more stable in the case of ZnS–SiO_2 films for both the UV and red bands compared to ZnS films without silica capping.

When the ZnS films without silica matrix were being aged in humid air, there was certain probability of passivation of S^{-2} vacancy by getting attached with –OH or ═O groups from air.

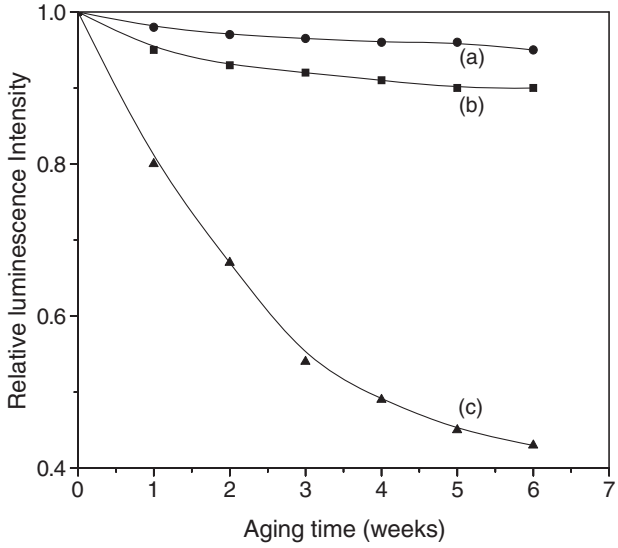

Fig. 7. Variation of relative intensity of luminescence with the aging time: (a) UV band of ZnS quantum dots embedded in silica films, (b) Red band of ZnS quantum dots embedded in silica films and (c) ZnS quantum dots without any silica coatings.

This process helped to decrease the population of the defect sites responsible for the blue emission, resulting in a decrease in the PL emission intensity. In the case of the silica-coated ZnS nanoparticles, the UV luminescence was coming from the defects related to the interstitial Zn or S atoms, not from the vacancy sites. Due to this fact, the intensity of the UV luminescence band remained practically constant with aging; whereas, the intensity of the red band decreased slightly since there was also a finite probability of passivation of the S vacancies generated due to S–Zn bond disruption under high temperature annealing.

4. Conclusions

Luminescent ZnS quantum dots were synthesized in thin film form with and without silica coating via a simple method using sol-gel technique. ZnS quantum dots without silica capping showed size-dependent blue emission related to the surface traps at room temperature. A qualitative approach was taken to explain the evolution of the emission peak with increasing annealing temperature. Under different excitations, ZnS quantum dots embedded in silica matrix showed two different emission bands — UV and red emissions. There was red shift in the UV band but blue shift in the red band with increasing annealing temperature of the films. The quantum dots embedded in silica matrix showed better resistance against degradation of luminescence quality with aging when they were exposed in some humid atmosphere.

Acknowledgement

One of the authors (B.B.) would like to thank Ramananda College, Bishnupur, India for providing leave to participate in this research work.

References

[1] S.K. Mandal, S. Chaudhuri, A.K. Pal, Thin Solid Films 30 (1992) 209.
[2] R. Thielsch, T. Böhme, H. Böttcher, Phys. Status Solidi, A 155 (1996) 157.
[3] W. Chen, Z. Wang, Z. Lin, L. Lin, J. Appl. Phys. 82 (1997) 3111.
[4] S.M. Scholtz, R. Vacassy, J. Dutta, H. Hoffmann, J. Appl. Phys. 83 (1998) 7860.
[5] J. Nanda, S. Sapra, D.D. Sarma, N. Chandrasekharan, G. Hodes, Chem. Mater. 12 (2000) 1018.
[6] M. Tan, W. Cai, L. Zhang, Appl. Phys. Lett. 71 (1997) 3697.
[7] V. Dhas, A. Zaban, A. Gedanken, Chem. Mater. 11 (1999) 806.
[8] S.B. Qadri, E.F. Skelton, A.D. Dinsmore, J.Z. Hu, W.J. Kim, C. Nelson, B.R. Ratna, J. Appl. Phys. 89 (2001) 115.
[9] S.B. Qadri, E.F. Skelton, D. Hsu, A.D. Dinsmore, J. Yang, H.F. Gray, B.R. Ratna, Phys. Rev., B 60 (1999) 9191.
[10] T. Sekikawa, H. Yao, T. Hayashi, T. Kobayashi, Solid State Commun. 83 (1992) 969.
[11] B. Bhattacharjee, D. Ganguli, S. Chaudhuri, A.K. Pal, Mater. Chem. Phys. 78 (2002) 372.
[12] H.-Y. Lu, S.-Y. Chu, S.-S. Tan, J. Cryst. Growth 269 (2004) 385.
[13] Y. Zhao, J.-M. Hong, J.-J. Zhu, J. Cryst. Growth 270 (2004) 438.
[14] Y. Ni, G. Yin, J. Hong, Z. Xu, Mater. Res. Bull. 39 (2004) 1967.
[15] J.F. Xu, W. Ji, J.Y. Lin, S.H. Tang, Y.W. Du, Appl. Phys., A 66 (1998) 639.
[16] J. Chen, Y. Li, Y. Wong, J. Wang, J. Yun, D. Cao, Mater. Res. Bull. 39 (2004) 185.
[17] D. Denzler, M. Olschewski, K. Sattler, J. Appl. Phys. 84 (1998) 2841.
[18] K. Kanemoto, H. Hosokawa, Y. Wada, K. Murakoshi, S. Yanagida, T. Sakata, H. Mori, M. Isikawa, H. Kobayashi, J. Chem. Soc., Faraday Trans. 92 (1996) 2401.
[19] C.B. Murray, D.J. Noris, M.G. Bawendi, J. Am. Chem. Soc. 115 (1993) 8706.
[20] R.N. Bhargava, D. Ghallaghr, X. Hong, A. Nurmikko, Phys. Rev. Lett. 72 (1994) 416.
[21] R. Menner, B. Dimmler, R.H. Mauch, H.W. Schock, J. Cryst. Growth 86 (1998) 906.
[22] Y. Zhu, C.L. Yuan, P.P. Ong, J. Appl. Phys. 92 (2002) 6828.
[23] K.W. Cheah, L. Xu, X. Huang, Nanotechnology 13 (2002) 238.
[24] W.G. Becker, A.J. Bard, J. Phys. Chem. 87 (1983) 4888.
[25] N. Murase, R. Jagannathan, Y. Kanematsu, M. Watanabe, A. Kurita, H. Hirata, T. Yazawa, T. Kushida, J. Phys. Chem., B 103 (1999) 754.
[26] S. Yanagida, M. Yoshida, T. Shiragami, C. Pac, H. Mori, H. Fujita, J. Phys. Chem. 94 (1990) 3104.
[27] N. Chestnoy, T.D. Harris, R. Hull, L.E. Brus, J. Phys. Chem. 90 (1986) 3393.
[28] J. Hu, Y. Bando, J. Zhan, D. Golberg, Adv. Funct. Mater. 15 (2005) 757.
[29] N. Kumbhojkar, V.V. Nikesh, A. Kshirsagar, S. Mahamuni, J. Appl. Phys. 88 (2000) 6260.